

Enhancing road image clarity with residual neural network dehazing model

Aerun Martin¹, Mohd Nazeri Kamaruddin¹, Zamani Md Sani², Hadhrami Abdul Ghani³

¹Faculty of Engineering and Technology, Multimedia University, Melaka, Malaysia

²Faculty of Technology and Electrical Engineering, Universiti Teknikal Malaysia Melaka, Melaka, Malaysia

³Faculty of Data Science and Computing, Universiti Malaysia Kelantan, Pengkalan Chepa, Malaysia

Article Info

Article history:

Received Dec 8, 2023

Revised Apr 6, 2024

Accepted Apr 17, 2024

Keywords:

Advanced driver assistance system

Deep learning

Dehazing algorithm

Image enhancement

Lane markers

ABSTRACT

Lane markers, or road markers, are the painted lines on a roadway that separate different lanes of traffic. Lane markers guide drivers and ensure orderly vehicle flow. They are essential for advanced driver assistance systems (ADAS), providing reference points for vehicle positioning on the road. These markers enable ADAS to give warnings, assistance, and automation features that enhance driver safety and convenience. However, unpredictable illumination, such as a foggy environment, can suppress marker visibility, impacting ADAS's performance. Deep learning-based methods are well-known for their superiority in handling various haze patterns. This paper presents a residual network (ResNet)-based deep learning model to improve road image clarity impacted by fog. The residual neural network dehaze model (RNN-D) utilises a joint loss function to produce haze-free images with improved lighting conditions and enhanced details. The model was trained, validated, and fine-tuned using hazy and corresponding non-hazy datasets to ensure that the model is quantitatively superior in the peak signal-to-noise ratio (PSNR) and the structural similarity index measure (SSIM). RNN-D achieved an average PSNR of 27.98 and SSIM of 0.8 on multiple open-sourced datasets. The proposed algorithm's superior performance and visually appealing results make it a powerful tool for real-world image dehazing applications.

This is an open access article under the [CC BY-SA](#) license.



Corresponding Author:

Mohd Nazeri Kamaruddin

Faculty of Engineering and Technology, Multimedia University (Melaka Campus)

St. Ayer Keroh Lama, Melaka-75450, Malaysia

Email: nazeri.kamaruddin@mmu.edu.my

1. INTRODUCTION

Natural atmospheric phenomena such as fog, haze, and smog impact the quality and visibility of road image features, especially on the lane marker information. Marker information is critical for accurate and precise classification of lane markers to improve the performance of the advanced driver assistance system (ADAS) [1]. As a result, developing effective and robust dehazing techniques has become critical to enhancing image quality in real-world scenarios. Traditional dehazing methods like contrast stretching [2], guided filtering [3], and dark channel priors (DCP) [4] are pioneering approaches towards image dehazing that accelerate the development of dehazing methods. However, these methods are rigid and only applicable to certain levels of fog, which are not practical for real-world scenarios with diverse haze patterns. These limitations have prompted the exploration of deep learning-based approaches, which have shown significant improvements in image dehazing [5], [6]. Residual neural networks (RNN) are one of the deep learning models popular for machine vision applications such as segmentation, object identification, and image classification.

Their ability to learn complex features with rapid training through skip connection makes them one of the competitive methodologies in recent dehazing techniques [7]. Leveraging the computational efficiency of residual network (ResNet), this paper proposes a ResNet-based dehazing methodology using atmospheric scattering estimation without explicit transmission map and atmospheric light estimation, which has been a prominent methodology in past studies. This approach demonstrates a significant improvement in peak signal-to-noise ratio (PSNR) and structural similarity index measure (SSIM) compared to state-of-the-art dehazing techniques on various haze patterns while maintaining the fine details of the original scene. The main contributions of this study are summarised as follows: i) novel ResNet-based dehazing methodology using the atmospheric scattering model (ASM) without the need to compute the transmission map and atmospheric light separately; and ii) validation and refinement of the loss function for enhancing the PSNR and SSIM of dehazed images.

The remainder of this paper is organised as follows. In section 2, related work on image dehazing techniques is reviewed. Section 3 presents the proposed ResNet-based dehazing algorithm. Section 4 details the experimental setup and evaluation of the method. Finally, section 5 concludes the paper and discusses potential future work.

2. RELATED WORK

There are two primary approaches to image dehazing: classical and deep-learning-based. Classical methods, such as the DCP [4], detect low-intensity pixels in haze-free areas and employ a haze imaging model to estimate the thickness of the haze and recover high-quality haze-free images. However, one limitation of DCP is the presence of halo artefacts around high-contrast edges in dehazed images, which can negatively affect overall visual quality. To address this issue, a guided filter [3] was proposed that applies local linear models to filter an image based on the content of the guidance image, whether it is the input image itself or a different image. The guided filter effectively performs edge-preserving smoothing, particularly near the edges, thereby mitigating halo artefacts. Additionally, contrast stretching [8] and histogram equalisation [9] have been proposed for the contrast enhancement of images due to haze removal by DCP. Contrast stretching aims to enhance contrast by extending the range of intensity values. On the other hand, histogram equalisation focuses on reshaping intensity value distributions for a more uniform spread. However, it is essential to acknowledge that applying histogram equalisation can introduce the risk of exacerbating noise and artefacts, mainly when dealing with foggy images subjected to illumination. Meng *et al.* [10] presented a methodology that efficiently combines boundary constraints and contextual regularisation to address these challenges. This approach effectively harnesses the synergy between boundary information and contextual coherence to achieve improved results in image dehazing. Li and Zheng [11] discussed an edge-based approach to single-image haze removal using adaptive contrast enhancement. This method utilises an edge-preserving filter to enhance the image's contrast while preserving edge information. The enhancement strength is adaptively adjusted based on the local contrast level to achieve improved results. Despite these efforts, traditional techniques often struggle to consistently generate high-quality haze-free images due to their limitations in dealing with diverse and challenging haze patterns.

Recent advances in deep-learning-based approaches have led to significant improvements in image dehazing, making them a powerful alternative for various applications. DehazeNet [5] is a groundbreaking deep learning-based approach that estimates atmospheric light and haze transmission maps from hazy images. However, a potential disadvantage of DehazeNet is the need for a refinement process to enhance the accuracy of the transmission map, which could add computational complexity. Building on the success of DehazeNet, Ren *et al.* [12] proposed a multi-scale convolutional neural network (CNN) that captures features at various levels of detail. This strategy effectively captures local and global contextual information, but it may still suffer from some loss of fine details due to the fixed receptive field sizes of convolutional filters. Denoising convolutional neural networks (DnCNN)-enhance [13] utilises residual learning and batch normalisation to enhance image optimisation. While this method achieves state-of-the-art results for various image restoration tasks, it might require substantial computational resources for training due to its deep network architecture. All-in-one dehazing network (AOD-Net) [6] is a comprehensive dehazing network that directly learns the mapping from hazy to haze-free images in a single step. The advantage of AOD-Net is its ability to eliminate the explicit calculation of the transmission map and atmospheric light, simplifying the dehazing process. However, a limitation of AOD-Net might be its reliance on large-scale datasets for training, which could be challenging to acquire in some cases. GridDehazeNet [14] leverages a grid structure and multi-scale data for enhanced dehazing performance. While this approach effectively handles complex haze patterns, it may still struggle with thick or dense scenes. Gated fusion network (GFN) [15] and its adaptive fusion of multi-scale features through gating mechanisms effectively emphasise informative features for improved dehazing performance. However, one potential limitation of this method is that the gating mechanism might require

careful tuning and might not generalise optimally across all hazy scenes. Kim *et al.* [16] presented a spatially adaptive atmospheric point-spread function (APSF) technique for dehazing road scene images. While this approach is practical for road scenes, it might face challenges in dealing with more diverse and complex natural scenes. The advantages of the new methods, such as AOD-Net and GFN, over past methods like DehazeNet and multi-scale CNN lie in their ability to handle haze removal in a single step without explicitly estimating transmission maps and atmospheric light. This streamlined approach simplifies the dehazing process and reduces computational complexity. Additionally, these newer methods incorporate adaptive feature fusion and gating mechanisms, enabling them to capture informative features more effectively and improve dehazing performance. In the streamline of the CNN network, Meng *et al.* [17] proposed a two-stream CNN or single-image dehazing. This network architecture comprises a spatial information feature stream and a high-level semantic feature stream. The spatial information feature stream preserves intricate details of the dehazed image, while the high-level semantic feature stream captures multi-scale structural features. An auxiliary module focused on spatial information is integrated between the feature streams. This module employs an attention mechanism to unify diverse information types, progressively restoring image clarity with semantic information. A parallel residual module enhances haze discrimination by dehazing feature differences across stages. The advancements in deep learning-based techniques have shown great promise in addressing complex haze patterns and significantly improving image dehazing results. However, it is essential to consider each method's specific requirements and limitations when applying them in different real-world scenarios.

ResNet [7] have gained popularity in various computer vision tasks, including image dehazing, due to their effective deep feature learning capabilities and ability to mitigate the vanishing gradient problem. Zhou *et al.* [18] proposed a ResNet-based model called a multi-scale residual network (MSRN) for single-image dehazing, which integrates multi-scale features from different network layers to capture haze distribution and scene details effectively. The model outperformed previous state-of-the-art methods in both quantitative and qualitative evaluations. Yi *et al.* [19] presented a dual residual network for single-image dehazing that combines separate residual networks to estimate transmission maps and atmospheric light. By utilising a joint loss function considering both transmission and atmospheric light estimations, DR-ResNet achieves improved dehazing performance. ResNet-based model known as the cascaded residual dense network (CRDN) [20] employs a cascaded structure to refine the dehazed result iteratively. These ResNet-based approaches showcase the versatility and effectiveness of residual learning in image dehazing tasks, adapting to different haze patterns and effectively removing haze while preserving scene details. In the realm of single-image dehazing, a prominent challenge in low-level computer vision, recent developments have introduced innovative approaches to address the complexities of the problem. Pyramid attention residual feature extraction network (PARFE-Net) [21] model combines a feature pyramid network to capture diverse image features across different scales and an attention-based resblock that strategically enhances crucial areas, improving output image quality. Research by Jiang *et al.* [22] is an end-to-end trainable, densely connected residual spatial and channel attention network that eliminates the need for explicit estimation of atmospheric parameters and employs a unique residual attention module to dynamically adjust feature weights, effectively focusing on regions of importance. Wang *et al.* [23] addresses domain shift issues between synthetic and real-world hazy images through the twofold multi-scale generative adversarial network (TMS-GAN) framework. This dual-stage training scheme comprises a haze-generation generative adversarial network (HgGAN) and a haze-removal generative adversarial network (HrGAN) working cooperatively to generate and remove haze, aided by structural advancements like a haze residual map and a multi-attention progressive fusion module (MAPFM) for effective feature fusion. These innovative approaches collectively push the boundaries of single-image dehazing, showcasing promising results and advancements over existing techniques.

With the increasing dehazing methods integrated with robust base networks such as CNN and ResNet, the end-to-end architecture with increased accuracy and less computation still has a high potential to tackle various haze patterns. This technique is more practical in real-world scenarios, requiring minimal time to process the hazy image and output high-quality dehaze images to yield better results and contribute to autonomous vehicles and ADAS's safety and efficiency.

3. METHOD

Hazy images often suffer colour deviation and low contrast due to selective absorption and light scattering, whose degradation is generally described by an ASM. In (1) represents the mathematical expression for the ASM.

$$I(x) = J(x)t(x) + A(1 - t(x)) \quad (1)$$

Where, $I(x)$ represents the observed hazy image, $J(x)$ represents the scene radiance or “clean image” required to recover, A represents the global atmospheric light, and $t(x)$ represents the transmission map. The

transmission map plays a crucial role in ASM. It determines how much light is attenuated and scattered when it travels through a hazy medium. In equation form, the transmission map can be expressed as (2):

$$t(x) = e^{-\beta d(x)} \quad (2)$$

Where β represents the scattering coefficient of the atmosphere, and $d(x)$ represents the distance between the object and the camera. The ASM is a fundamental concept used to understand hazy image formation and is commonly employed in image restoration and enhancement. The clean image $J(x)$ can be obtained from the hazy image $I(x)$ using the transmission map $t(x)$ and atmospheric light A according to (3) [6]:

$$J(x) = \frac{1}{t(x)}I(x) - A\frac{1}{t(x)} + A \quad (3)$$

The algorithm offers a significant advantage by minimising the reconstruction error $K(x)$ directly on the clean image $J(x)$, without the need for separate estimation of the transmission map $t(x)$ and atmospheric light A . By combining the estimation of $t(x)$ and A , they effectively reduce the reconstruction error at the pixel level of the image. This was accomplished using (4):

$$J(x) = K(x)I(x) + K(x) + b \quad (4)$$

where

$$K(x) = \frac{\frac{1}{t(x)}(I(x)-A)+(A-b)}{I(x)-1} \quad (5)$$

b represents a constant bias term in the algorithm. This term plays a role in adjusting the reconstruction error, contributing to the overall accuracy of the dehazing process. The joint estimation process compensates for inaccuracies in other hyperparameters, such as gamma correction, enhancing overall image quality.

The ResNet architecture was chosen due to its ability to train deep networks by alleviating the vanishing gradient problem. The network is trained using the Adam optimiser for ten epochs, with a learning rate $1e^{-4}$. The batch size is set to 8. The Adam optimiser, short for adaptive moment estimation, has become a preferred choice in deep learning due to its distinct advantages. At its core, Adam seamlessly combines the strengths of two popular extensions of stochastic gradient descent: momentum and root mean square propagation (RMSprop). While momentum leverages past gradients to smooth out the update process, RMSprop dynamically adjusts the learning rate based on recent gradient magnitudes. This blend results in per-parameter adaptive learning rates, making Adam particularly effective for problems with sparse gradients, which is standard in computer vision. Another pivotal feature of Adam is its bias-correction mechanism, which corrects the initial zero bias in its moving averages, ensuring a more accurate convergence.

The ResNet architecture is based on its unique residual block structure. Each block consists of two convolutional layers, followed by batch normalisation and rectified linear unit (ReLU) activation. The first layer uses a 1×1 kernel with stride s , while the second layer uses a 3×3 kernel with a stride of 1. The output is augmented by an integral shortcut connection, which includes a 1×1 convolutional layer aligned with the block's filter count and batch normalisation. This design allows the network to learn identity functions, preventing performance degradation when adding layers. The network starts with a 7×7 kernel, stride 2, and a 2D convolutional layer, followed by batch normalisation and ReLU activation. A 3×3 kernel follows this, stride two max pooling. Subsequent stages consist of multiple residual blocks, increasing the filter count while reducing spatial dimensions. After each stage, the filter count doubles while the dimensions halve. The network reverses the spatial reduction using transpose convolutional layers for upsampling, followed by batch normalisation and ReLU activation. The number of filters in these layers decreases similarly to the initial stages. The final layer is a 3-filter convolutional layer that matches the input image channels with batch normalisation. A specific step for haze removal combines the output of the final layer with the original input, subtracting the estimated haze from the hazy image to restore clarity.

The objective function for training the network is the mean squared error (MSE) between the dehazed output image and the corresponding ground-truth clear image. The output images are resized to match the size of the ground truth image before computing the MSE. The Adam optimisation algorithm is used to minimise the loss. MSE is commonly used for regression tasks due to its simplicity, emphasis on more significant errors, and smooth gradient properties, which make it suitable for optimisation. In applications like image haze removal, the goal is to minimise the deviation between the dehazed output and the precise reference image. MSE naturally quantifies this deviation by calculating the average squared difference between the two. It is

penalisation of more significant errors ensures that the model aims for precision in haze removal, which is crucial for image clarity. The MSE equation is as (6):

$$MSE = \frac{\sum_{i=1}^n (y_i - \hat{y}_i)^2}{n} \quad (6)$$

To address the issue of exploding gradients often encountered in deep networks, the paper implemented gradient clipping by limiting the L2 norm of the gradients to 0.1 after computation. After training for ten epochs, the residual neural network dehaze (RNN-D) processed hazy images and generated results from its final layer. The network consisted of 101 layers with 8,911,369 parameters and was customised to handle specific haze characteristics. Unlike generic architectures, the tailored layers effectively addressed the impact of haze on contrast, colour, and detail. By utilising residual blocks, the network learned intricate representations while preserving important input information through skip connections, which aided in recovering fine details. Upsampling using transpose convolutional layers retained crucial spatial information necessary to restore original textures and details obscured by haze. The architecture of the RNN-D is shown in Figure 1.

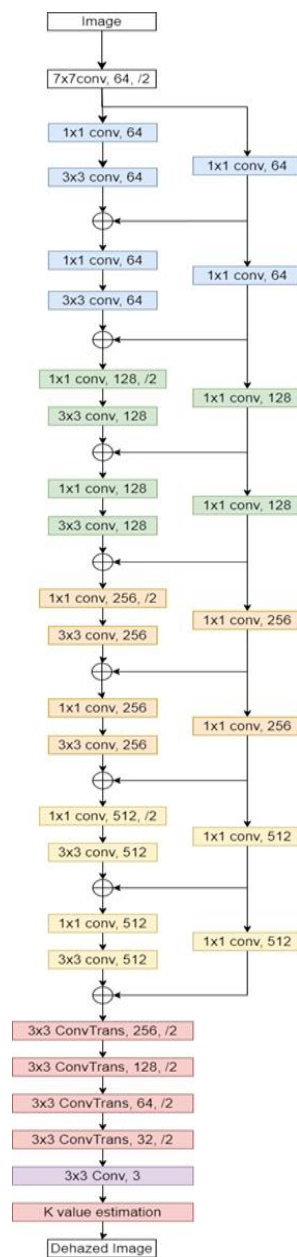


Figure 1. ResNet-based dehazing architecture with k-estimation for improved image clarity

4. RESULTS AND DISCUSSION

Access to high-quality training data is crucial for effective training models and achieving robust and accurate dehazing results [22]. This study utilises the NYU2 dataset to overcome this challenge for training purposes. The NYU2 dataset provides precise training data, allowing the model to learn effectively and produce enhanced results in image dehazing tasks [19], [24]. The training set consists of 27,256 images from the NYU2 dataset, while the test set includes 3,170 non-overlapping images. These datasets cover diverse indoor scenes with varying levels of haze. However, it is essential to note that the NYU2 dataset primarily focuses on indoor scenes. When these models are tested on outdoor datasets, such as those containing roads, accuracy may decrease due to the domain shift between indoor and outdoor images. Outdoor images often exhibit different lighting conditions and atmospheric effects compared to the indoor dataset, impacting the model's performance. The training sets were expanded to include the RESIDE dataset to address this limitation and improve the model's adaptability to a broader range of environments [25]. The RESIDE dataset provides a more diverse set of images for training, specifically the outdoor training set (OTS), which consists of 72,135 hazy and corresponding haze-free images. It was compared to eight state-of-the-art methods using 49 clean images augmented with synthetic haze to evaluate the method's performance. To ensure a fair comparison, 1,400 training images from the NYU2 dataset were excluded. The evaluation utilised two standard metrics: SSIM and PSNR [26].

$$PSNR = 10 \log_{10} \frac{\text{Squared Max possible Pixel}}{\text{Mean Squared Error}} \quad (7)$$

$$SSIM (DH, GT) = \frac{(2\mu_{DH}\mu_{GT} + K_1)(2\sigma_{DH,GT} + K_2)}{(\mu_{DH}^2 + \mu_{GT}^2 + K_1)(\sigma_{DH}^2 + \sigma_{GT}^2 + K_2)} \quad (8)$$

During the evaluation, three prior-based methods [4], [10], [27] and five learning-based methods [5], [6], [12], [15], [28] were considered for comparison. The first baseline approach, DCP, estimates a haze-free image using the local minimum statistics in the input image's haze-relevant channel. Boundary-constrained context regularisation (BCCR) combines contextual information and gradients to estimate the transmission map. The nonlocal image dehazing (NLD) algorithm considers nonlocal self-similarity and texture details during dehazing. Among the learning-based methods, color attenuation prior (CAP) employs a linear model based on the assumption of colour consistency across different regions. DehazeNet and multi-scale convolutional neural network (MSCNN) are CNN-based methods that learn the mapping between hazy inputs and their transmission. AOD-Net integrates transmission and atmospheric light into a new variable for haze-free image estimation. GFN uses a fusion-based strategy that incorporates white balance (WB), contrast enhancement (CE), and gamma correction (GC) to derive confidence maps. These maps are then used to blend information and preserve regions with improved visibility, resulting in the final dehazed image. A comparative analysis of various dehazing techniques, including prior-based methods and learning-based methods, was conducted, and compared with RNN-D. The results showed that prior-based methods tend to overestimate the haze thickness, leading to darker, dehazed images with colour distortions in certain regions. Although CAP, DehazeNet, MSCNN, and AOD-Net produced results closer to the ground truth, residual haze remained in the dehazed images. On the other hand, the RNN-D approach and GFN produced dehazed images that closely resembled the ground truth and demonstrated superior performance. The qualitative analysis is shown in Figure 2.

Based on the quantitative analysis in Table 1, RNN-D outperformed the other methods in PSNR values, indicating higher image quality. The method effectively reduces haze, resulting in a higher PSNR and the production of dehazed images that closely align with the ground truth. However, it is important to note that the approach may not consistently outperform other methods in terms of SSIM for all fog levels. This could be due to limitations in capturing structural information. SSIM measures structural similarity and considers luminance, contrast, and structure. RNN-D may be less effective in preserving structural information, leading to lower SSIM values at certain fog levels. Nevertheless, the approach generates visually appealing dehazed images with fewer colour distortions and demonstrates superior image quality based on PSNR values. This effectively reduces haze, producing high-quality dehazed images that closely match the ground truth.

The performance of RNN-D was further evaluated on the RESIDE dataset, which includes indoor and outdoor images with four state-of-the-art image dehazing algorithms (DCP, AOD-Net, DehazeNet, and GFN). Figure 3 visually compares the algorithms for indoor and outdoor scenes. DCP exhibits significant colour distortion and loss of detail, while AOD-Net fails to obliterate haze and produces low-brightness images. DehazeNet tends to overcompensate for brightness relative to the ground truth. In contrast, RNN-D demonstrates remarkable accuracy in recovering details, particularly in row 4, where it successfully restores the towers in the depth of the image. The results obtained by the other algorithms are unsatisfactory in comparison, highlighting the superior performance of RNN-D in terms of realistic image details and colour

fidelity. Table 2 summarises the PSNR and SSIM for indoor and outdoor scenes. RNN-D demonstrates superior performance, achieving significantly higher PSNR values than the other methods. Specifically, it achieves PSNR values of 28.87 and 28.39 for indoor and outdoor scenes, respectively, surpassing the results of the other algorithms. In conclusion, RNN-D outperforms state-of-the-art dehazing algorithms quantitatively and qualitatively, restoring clear and natural images from hazy scenes.

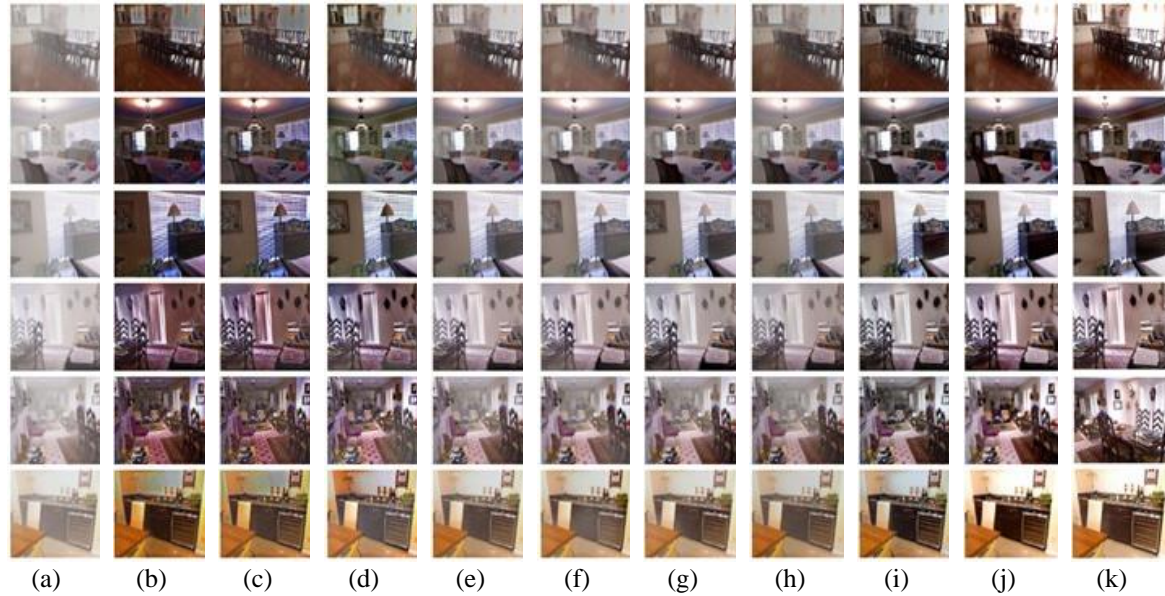


Figure 2. The dehazed results on the synthetic dataset (a) hazy input, (b) DCP [4], (c) BCCR [10], (d) NLD [27], (e) CAP [28], (f) MSCNN [12], (g) Dehaze Net [5], (h) AOD-Net [6], (i) GFN [15], (j) RNN-D, and (k) ground truths

Table 1. Average PSNR and SSIM values of dehazed results on NYU2 dataset

Evaluation Papers	PSNR/SSIM								
	DCP [4]	BCCR [10]	NLD [27]	CAP [28]	MSCNN [12]	DehazeNet [5]	AOD-Net [6]	GFN(G) [15]	Proposed
Light	18.74/0.77	17.72/0.76	18.61/0.71	21.92/0.83	22.34/0.82	24.87/0.84	22.64/0.85	24.78/0.85	27.97/0.85
Medium	18.68/0.77	17.54/0.75	18.47/0.70	21.40/0.82	21.21/0.80	23.37/0.83	21.33/0.84	23.68/0.84	27.96/0.78
Heavy	18.67/0.77	17.43/0.75	18.21/0.70	20.21/0.80	20.51/0.79	21.98/0.82	20.24/0.81	22.32/0.83	27.98/0.80
Random	18.58/0.77	17.35/0.75	18.28/0.71	19.99/0.78	20.01/0.78	20.97/0.80	19.36/0.78	22.41/0.81	28.00/0.77

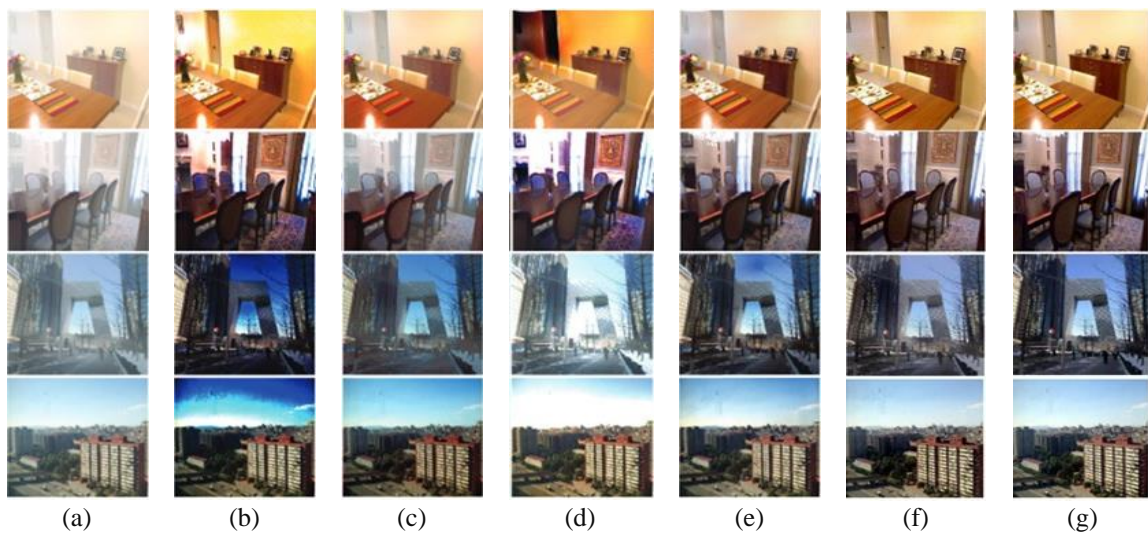


Figure 3. Indoor and outdoor results in SOTS: (a) hazy input, (b) DCP [4], (c) AOD-Net [6], (d) DehazeNet [5], (e) GFN [16], (f) RNN-D, and (g) ground truth

Table 2. Quantitative comparisons of SOTS for different methods

Methods	Indoor		Outdoor	
	PSNR	SSIM	PSNR	SSIM
DCP [4]	16.62	0.82	19.13	0.81
AOD-Net [6]	19.06	0.85	20.29	0.88
DehazeNet [5]	21.14	0.85	22.46	0.85
GFN [15]	22.30	0.88	21.55	0.84
RNN-D	28.87	0.83	28.39	0.82

Since the developed model performed well in the indoor and outdoor datasets, it was evaluated for its robustness in road datasets from the Frida and Frida 2 Datasets. These datasets contain a diverse range of road images with different haze levels, allowing for a comprehensive assessment of the method's effectiveness under various conditions and a comparison with traditional algorithms. The evaluation included qualitative and quantitative analysis using the SSIM and PSNR, following a similar approach in assessing the RESIDE and NYU2 datasets to ensure consistency and comparability. Qualitative highlighted the differences between the proposed method and previous approaches, focusing on the realistic representation of image details and colour accuracy in road images. Figure 4 shows the effectiveness of the proposed algorithm compared to earlier approaches on synthetic images from the FRIDA and FRIDA 2 datasets. Among the conventional methods, the DCP demonstrated the best performance in removing the four types of haze. The proposed method achieved results comparable to the DCP's, but some road colour distortion was observed in synthetic images. In the case of heterogeneous haze, the proposed method, along with the APSF and DCP, effectively dehazed the images and revealed buildings with more clarity than other methods. The patch map and homography-based local dehazing (PMHLD) method performed well overall but encountered difficulties in dense haze areas with cloudy environments. The CAP algorithm caused a decrease in saturation in achromatic areas with objects such as cars and roads. The APSF method, like the proposed technique, successfully removed all four types of haze without causing any colour change in objects within the road scene. The quantitative measurements presented in Table 3 provide quantitative evidence of the effectiveness of the RNN-D method compared to other methods. RNN-D achieved a PSNR score of 27.799 dB, an SSIM score of 0.584 on the FRIDA dataset, a PSNR score of 28.412 dB, and an SSIM score of 0.73 on the FRIDA2 dataset.

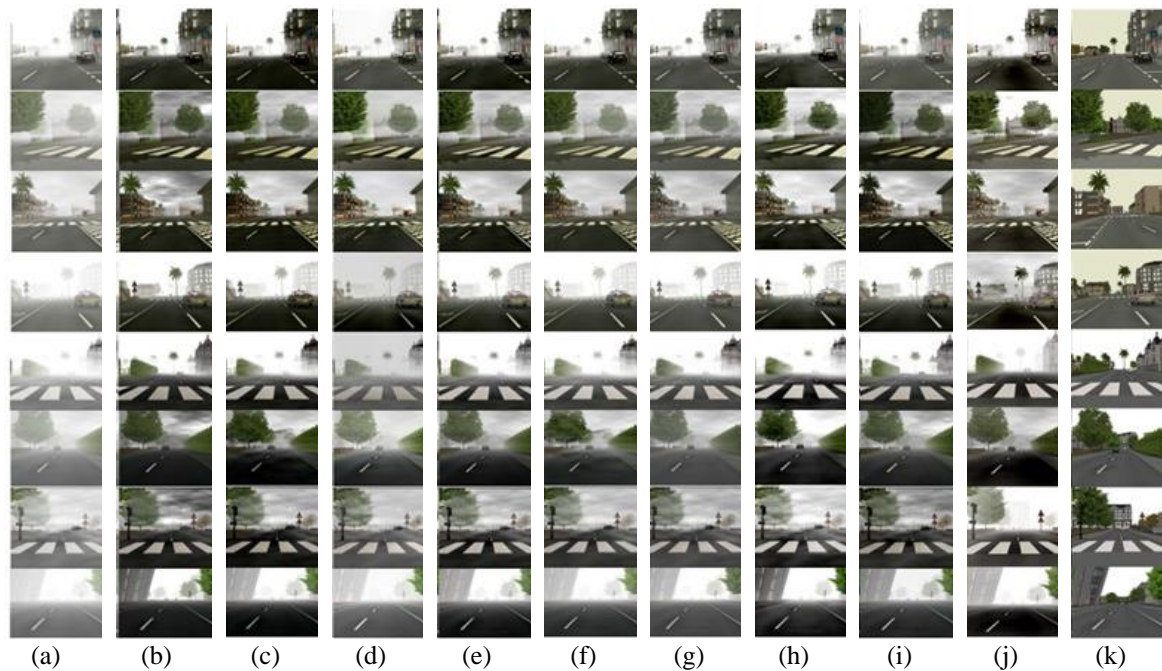


























Figure 4. Qualitative comparison of the FRIDA and FRIDA2 datasets: (a) hazy input, (b) DCP [4], (c) CAP [29], (d) DEFADE [30], (e) DehazeNet [5], (f) AOD-Net [6], (g) AMEF [31], (h) PMHLD [32], (i) APSF [33], (j) RNN-D, and (k) ground truths

Table 3. Quantitative comparisons on FRIDA and FRIDA2 datasets

Dataset	Metrics	Hazy	DCP [4]	CAP [29]	DEFADE [30]	DehazeNet [5]	AOD- Net [6]	AMEF [31]	PMHLD [32]	ASMF [33]	RNN- D
FRIDA (76 samples)	SSIM	0.616	0.6	0.522	0.566	0.614	0.629	0.68	0.563	0.693	0.584
	PSNR	11.167	13.316	12.494	13.226	12.926	13.229	1.237	12.697	13.875	27.799
FRIDA2 (264 samples)	SSIM	0.737	0.642	0.334	0.756	0.662	0.44	0.787	0.656	0.803	0.73
	PSNR	10.472	11.638	8.826	12.048	11.8	9.749	12.713	11.695	12.549	28.412

The availability of the original images in the synthetic dataset allows for more accurate comparisons of the haze removal achieved by each algorithm. However, analysing the algorithm using real road datasets is critical to identify its effectiveness. Thus, the algorithm was further evaluated on the cityscape road dataset to assess its robustness in dehazing actual road images with road markers. Table 4 presents a qualitative analysis of the model's performance on selected images from the dataset since there are no haze-free images for quantitative analysis. The dehazed images using the RNN-D algorithm significantly improve the visibility of road markers. This enhancement is attributed to the increased contrast differentiation between the road surface and the markers. The reduced contrast between these elements can lead to classification errors in foggy conditions. However, the RNN-D dehazing technique enhances the feature extraction capabilities specific to road markers, reducing the likelihood of misclassification.

Table 4. Qualitative analysis of RNN-D effectiveness on cityscape real road dataset

Image no	Actual image	Dehazed images	Image no	Actual image	Dehazed images
1			7		
2			8		
3			9		
4			10		
5			11		
6			12		

5. CONCLUSION

In conclusion, the proposed ResNet-based dehazing algorithm, RNN-D, has demonstrated excellent performance on various datasets, including NYU2, RESIDE, FRIDA, and FRIDA2. It outperformed existing state-of-the-art dehazing algorithms in terms of objective metrics such as PSNR and SSIM, as well as subjective evaluations based on visual quality. The algorithm effectively recovers clear and natural images from hazy scenes, even under challenging conditions with varying degrees and types of haze. This makes it a promising solution for enhancing image quality in adverse weather situations. The quantitative analysis showed that the proposed algorithm outperformed existing techniques on multiple datasets, including SOTS: indoor, outdoor, NYU2, FRIDA, and FRIDA2. Additionally, the validation on real images demonstrated high contrast between

road markers and the road surface, which enhances feature extraction for road marker classification. This has significant implications for applications such as autonomous driving, where image quality and accuracy are crucial for safety and reliability. The proposed algorithm's superior performance and visually appealing results make it a powerful tool for image-dehazing applications. Future work could discuss the technique for classifying road markers extracted from dehazed images, further enhancing the classification algorithm and reducing errors caused by foggy illumination.

ACKNOWLEDGEMENTS

The authors express their gratitude to the Malaysian government for sponsoring this project and those who have contributed to completing this paper directly or indirectly. The funding of this research is provided by a grant from the Malaysian Ministry of Higher Education (FRGS/1/2019/TK04/MMU/02/2).




REFERENCES

- [1] H. A. Ghani *et al.*, "Advances in lane marking detection algorithms for all-weather conditions," *International Journal of Electrical and Computer Engineering (IJECE)*, vol. 11, no. 4, pp. 3365–3373, Aug. 2021, doi: 10.11591/ijece.v11i4.pp3365-3373.
- [2] J.-P. Tarel and N. Hautiere, "Fast visibility restoration from a single color or gray level image," in *2009 IEEE 12th International Conference on Computer Vision*, IEEE, Sep. 2009, pp. 2201–2208, doi: 10.1109/ICCV.2009.5459251.
- [3] K. He, J. Sun, and X. Tang, "Guided image filtering," *IEEE Transactions on Pattern Analysis and Machine Intelligence*, vol. 35, no. 6, pp. 1397–1409, Jun. 2013, doi: 10.1109/TPAMI.2012.213.
- [4] H. Kaiming, S. Jian, and T. Xiaoou, "Single image haze removal using dark channel prior," in *2009 IEEE Conference on Computer Vision and Pattern Recognition*, IEEE, Jun. 2009, pp. 1956–1963, doi: 10.1109/CVPR.2009.5206515.
- [5] B. Cai, X. Xu, K. Jia, C. Qing, and D. Tao, "DehazeNet: an end-to-end system for single image haze removal," *IEEE Transactions on Image Processing*, vol. 25, no. 11, pp. 5187–5198, Nov. 2016, doi: 10.1109/TIP.2016.2598681.
- [6] B. Li, X. Peng, Z. Wang, J. Xu, and D. Feng, "AOD-Net: all-in-one dehazing network," in *2017 IEEE International Conference on Computer Vision (ICCV)*, IEEE, Oct. 2017, pp. 4780–4788, doi: 10.1109/ICCV.2017.511.
- [7] S. Zhang and F. He, "DRCN: learning deep residual convolutional dehazing networks," *The Visual Computer*, vol. 36, no. 9, pp. 1797–1808, Sep. 2020, doi: 10.1007/s00371-019-01774-8.
- [8] Erwin, "Improving retinal image quality using the contrast stretching, histogram equalization, and CLAHE methods with median filters," *International Journal of Image, Graphics and Signal Processing*, vol. 12, no. 2, pp. 30–41, Apr. 2020, doi: 10.5815/ijigsp.2020.02.04.
- [9] Z. M. Sani, L. J. Chuan, T. A. Izzudin, H. A. Ghani, and A. Martin, "Urban Road marker classification using histogram of oriented gradient and local binary pattern with artificial neural network," in *Proceedings of International Conference on Emerging Technologies and Intelligent Systems: ICETIS 2021*, 2022, pp. 126–135, doi: 10.1007/978-3-030-82616-1_12.
- [10] G. Meng, Y. Wang, J. Duan, S. Xiang, and C. Pan, "Efficient image dehazing with boundary constraint and contextual regularization," in *The IEEE International Conference on Computer Vision*, 2013, pp. 617–624, doi: 10.1109/ICCV.2013.82.
- [11] Z. Li and J. Zheng, "Edge-preserving decomposition-based single image haze removal," *IEEE Transactions on Image Processing*, vol. 24, no. 12, pp. 5432–5441, Dec. 2015, doi: 10.1109/TIP.2015.2482903.
- [12] W. Ren, S. Liu, H. Zhang, J. Pan, X. Cao, and M.-H. Yang, "Single image dehazing via multi-scale convolutional neural networks," in *Computer Vision-ECCV 2016: 14th European Conference, Amsterdam, The Netherlands, October 11-14, 2016, Proceedings, Part II 14*, 2016, pp. 154–169, doi: 10.1007/978-3-319-46475-6_10.
- [13] M. M. Ho, J. Zhou, and G. He, "RR-DnCNN v2.0: enhanced restoration-reconstruction deep neural network for down-sampling-based video coding," *IEEE Transactions on Image Processing*, vol. 30, pp. 1702–1715, 2021, doi: 10.1109/TIP.2020.3046872.
- [14] X. Liu, Y. Ma, Z. Shi, and J. Chen, "GridDehazeNet: attention-based multi-scale network for image dehazing," in *2019 IEEE/CVF International Conference on Computer Vision (ICCV)*, IEEE, Oct. 2019, pp. 7313–7322, doi: 10.1109/ICCV.2019.00741.
- [15] W. Ren *et al.*, "Gated fusion network for single image dehazing," in *2018 IEEE/CVF Conference on Computer Vision and Pattern Recognition*, IEEE, Jun. 2018, pp. 3253–3261, doi: 10.1109/CVPR.2018.00343.
- [16] M. Kim, S. Hong, H. Lee, and M. G. Kang, "Single image dehazing of road scenes using spatially adaptive atmospheric point spread function," *IEEE Access*, vol. 9, pp. 76135–76152, 2021, doi: 10.1109/ACCESS.2021.3082175.
- [17] J. Meng, Y. Li, H. Liang, and Y. Ma, "Single image dehazing based on two-stream convolutional neural network," *Journal of Artificial Intelligence and Technology*, Jun. 2022, doi: 10.37965/jait.2022.0110.
- [18] J. Zhou, C. T. Leong, and C. Li, "Multi-scale and attention residual network for single image dehazing," in *2021 6th International Conference on Intelligent Computing and Signal Processing (ICSP)*, Apr. 2021, pp. 483–487, doi: 10.1109/ICSP51882.2021.9408801.
- [19] W. Yi, L. Dong, M. Liu, Y. Zhao, M. Hui, and L. Kong, "DCNet: dual-cascade network for single image dehazing," *Neural Computing and Applications*, vol. 34, no. 19, pp. 16771–16783, Oct. 2022, doi: 10.1007/s00521-022-07319-w.
- [20] Y. Yang, C. Hou, H. Huang, Z. Zhang, and G. Xie, "Cascaded deep residual learning network for single image dehazing," *Multimedia Systems*, vol. 29, no. 4, pp. 2037–2048, Aug. 2023, doi: 10.1007/s00530-023-01087-w.
- [21] J. Zhou, C. T. Leong, and C. Li, "Multi-scale and attention residual network for single image dehazing," in *2021 6th International Conference on Intelligent Computing and Signal Processing (ICSP)*, IEEE, Apr. 2021, pp. 483–487, doi: 10.1109/ICSP51882.2021.9408801.
- [22] X. Jiang, C. Zhao, M. Zhu, Z. Hao, and W. Gao, "Residual spatial and channel attention networks for single image dehazing," *Sensors*, vol. 21, no. 23, p. 7922, Nov. 2021, doi: 10.3390/s21237922.
- [23] P. Wang, H. Zhu, H. Huang, H. Zhang, and N. Wang, "TMS-GAN: a twofold multi-scale generative adversarial network for single image dehazing," *IEEE Transactions on Circuits and Systems for Video Technology*, vol. 32, no. 5, pp. 2760–2772, May 2022, doi: 10.1109/TCSVT.2021.3097713.
- [24] C. Y. Jeong, K. Moon, and M. Kim, "An end-to-end deep learning approach for real-time single image dehazing," *Journal of Real-Time Image Processing*, vol. 20, no. 1, p. 12, Feb. 2023, doi: 10.1007/s11554-023-01270-2.
- [25] B. Li *et al.*, "Benchmarking single-image dehazing and beyond," *IEEE Transactions on Image Processing*, vol. 28, no. 1, pp. 492–505, Jan. 2019, doi: 10.1109/TIP.2018.2867951.




- [26] Z. Wang, A. C. Bovik, H. R. Sheikh, and E. P. Simoncelli, "Image quality assessment: from error visibility to structural similarity," *IEEE Transactions on Image Processing*, vol. 13, no. 4, pp. 600–612, Apr. 2004, doi: 10.1109/TIP.2003.819861.
- [27] D. Berman, T. Treibitz, and S. Avidan, "Non-local image dehazing," in *2016 IEEE Conference on Computer Vision and Pattern Recognition (CVPR)*, IEEE, Jun. 2016, pp. 1674–1682, doi: 10.1109/CVPR.2016.185.
- [28] Z. Qingsong, M. Jiaming, and S. Ling, "A fast single image haze removal algorithm using color attenuation prior," *IEEE Transactions on Image Processing*, vol. 24, no. 11, pp. 3522–3533, Nov. 2015, doi: 10.1109/TIP.2015.2446191.
- [29] R. Fattal, "Dehazing using color-lines," *ACM Transactions on Graphics (TOG)*, vol. 34, no. 1, pp. 1–14, Dec. 2014, doi: 10.1145/2651362.
- [30] L. Kwon Choi, J. You, and A. C. Bovik, "Referenceless prediction of perceptual fog density and perceptual image defogging," *IEEE Transactions on Image Processing*, vol. 24, no. 11, pp. 3888–3901, Nov. 2015, doi: 10.1109/TIP.2015.2456502.
- [31] A. Galdran, "Image dehazing by artificial multiple-exposure image fusion," *Signal Processing*, vol. 149, pp. 135–147, Aug. 2018, doi: 10.1016/j.sigpro.2018.03.008.
- [32] W.-T. Chen, H.-Y. Fang, J.-J. Ding, and S.-Y. Kuo, "PMHLD: patch map-based hybrid learning dehazenet for single image haze removal," *IEEE Transactions on Image Processing*, vol. 29, pp. 6773–6788, 2020, doi: 10.1109/TIP.2020.2993407.
- [33] M. Kim, S. Hong, H. Lee and M. G. Kang, "Single image dehazing of road scenes using spatially adaptive atmospheric point spread function," in *IEEE Access*, vol. 9, pp. 76135–76152, 2021, doi: 10.1109/ACCESS.2021.3082175.

BIOGRAPHIES OF AUTHORS






Aerun Martin    holds received the Bachelor in Mechatronics from University Technical Malaysia Melaka and currently pursuing Master's degree in Engineering Technology from Multimedia University. His current area of interest is image processing, machine learning, and deep learning. He can be contacted at email: aerunmartin@gmail.com.






Mohd Nazeri Kamaruddin    holds a Bachelor's degree in Electronics Engineering majoring in Telecommunications from Multimedia University, Malaysia in 2003 and the Master's degree in Telecommunications Engineering from University of Melbourne, Australia in 2005. Currently, he is an academic staff at the Faculty of Engineering and Technology, Multimedia University. His research interests include radio propagation for indoor and outdoor, ray tracing algorithm, RFID, antenna design, evolutionary and heuristic optimization, image processing and neural networks. He can be contacted at email: nazeri.kamaruddin@mmu.edu.my.



Zamani Md Sani    received his degree in 2000 from Universiti Sains Malaysia. He worked at Intel Malaysia Kulim for six years and obtained his Master's at the same university in 2009. Later, he joined education at Universiti Teknikal Malaysia Melaka and obtained his Ph.D. from Multimedia University in 2020. His research interest is in image processing and artificial intelligence. He can be contacted at email: zamanisani@utem.edu.my.



Hadhrami Abdul Ghani    received his bachelor's degree in electronics engineering from Multimedia University Malaysia (MMU) in 2002. In 2004, he completed his master's degree in telecommunication engineering at the University of Melbourne. He then pursued his PhD in intelligent network systems at Imperial College London and completed it in 2011. His current research interests are advanced communications, network security and computer vision. He is a senior lecturer at the Faculty of Data Science and Computing, Universiti Malaysia Kelantan. He can be contacted at email: hadhrami.ag@umk.edu.my.